PHYSICAL REVIEW B VOLUME 8, NUMBER 1 1 JULY 1973

Temperature Dependence of Multiphonon Nonradiative Decay at an Isolated Impurity Center

M. D. Sturge
Bell Laboratories, Murray Hill, New Jersey 07974
(Received 14 February 1973)

The fluorescent lifetime of the $^4T_2$ excited state of Co^{2+} in $KMgF_3$ is measured from 1.6 to 550 °K. The radiative lifetime is calculated from the oscillator strength of the $^4T_1 \rightarrow {}^4T_2$ transition and the nonradiative decay rate deduced. This varies over four orders of magnitude. Its temperature dependence is in good agreement with that predicted for linear coupling to a continuum of harmonic phonons, with parameters deduced from the zero-phonon and one-phonon spectrum. To obtain agreement, the decrease of the energy gap with temperature, which is primarily due to anharmonicity, must be taken into account. The absolute value of the nonradiative decay rate is two orders of magnitude smaller than predicted by the model. It is shown that this discrepancy, and the much more dramatic discrepancy found in ruby, can reasonably be attributed to anharmonicity. The continuum model is compared with a discrete-frequency model, and it is shown that the "effective frequency" of the continuum, however, defined, is closer to its mean frequency than to its maximum.

I. INTRODUCTION

The mechanism of nonradiative transitions in molecules, and in isolated centers in crystals, has attracted much theoretical attention recently.[1] A simple model can account for the nonradiative transition rates observed in some transition-metal- and rare-earth-ion centers.[2,3] However, the same model fails completely in other cases; for instance, the nonradiative decay rate of the ^2E state of ruby is a factor of order 10^{17} faster[4] than predicted. More attention has been paid to the absolute value of the transition rate (usually near 0 °K), than to its temperature dependence, which might, however, be expected to provide a more critical test of theory. Measurements of the temperature dependence of nonradiative transitions of Er^{3+} and Ho^{3+} in LaF_3 and Dy^{3+} in $LaBr_3$ have been made over a limited range[3] without uncovering any gross failure of the theory. Measurements on d^3 systems up to quite high temperatures[5] have given little information about nonradiative decay rates, since the change in lifetime is dominated by the rapid variation of the radiative decay rate as different excited electronic states are occupied.

We report here measurements of the $^4T_2 \rightarrow {}^4T_1$ fluorescent lifetime of Co^{2+} dilutely incorporated into $KMgF_3$. The energy-level diagram for this d^7 system is shown in Fig. 1. The spin-orbit splitting in the lowest vibronic level of $^4T_2$ is strongly quenched by the dynamic Jahn-Teller effect,[6] leaving the residual splittings shown.

In $KMgF_3$, as in other octahedral fluoride hosts, Co^{2+} fluoresces strongly in the infrared under excitation in any of its stronger absorption bands. The emission spectrum at very low temperatures (below 5 °K) is shown in Fig. 2. It consists of a sharp no-phonon line at 6900 cm^{-1} corresponding to the $^4T_2(\Gamma_6) \rightarrow {}^4T_1(\Gamma_6)$ transition, and a broad and strongly structured vibronic sideband peaking at about 6000 cm^{-1}. Superimposed on the sideband is a strong no-phonon line at 5950 cm^{-1}. This is the $^4T_2(\Gamma_6) \rightarrow {}^4T_1(\frac{5}{2}\Gamma_8)$ transition, which has been made to lase under flash-tube excitation.[7] The one-phonon structure associated with each of these no-phonon lines has a strong resemblance to that observed in the fluorescence of V^{2+} and Ni^{2+} in $KMgF_3$,[8] although the spin-orbit splitting of the

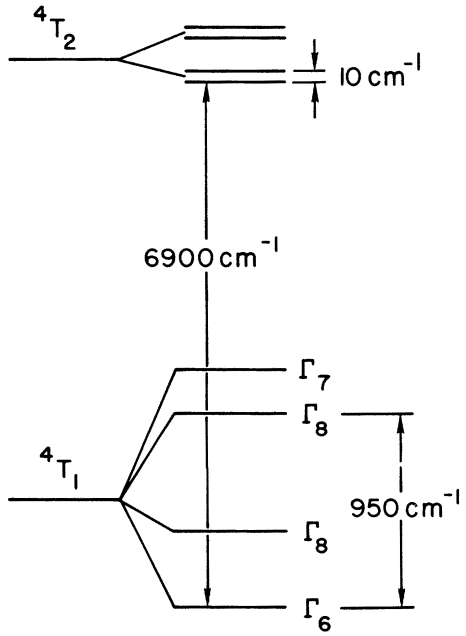

FIG. 1. Energy-level diagram of Co^{2+} in the Mg^{2+} site of $KMgF_3$ (O_h symmetry). The order of the levels in the $^4T_2$ term is the same as in $^4T_1$.

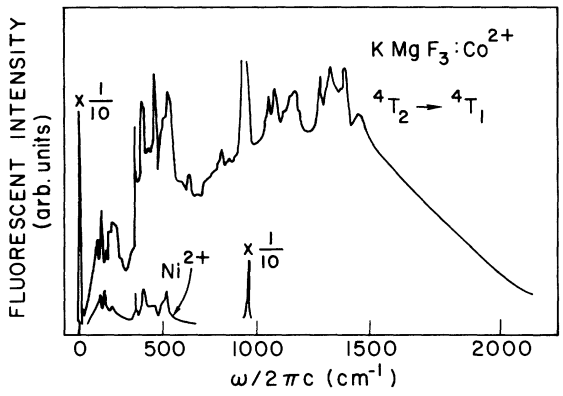

FIG. 2. Infrared emission spectra of Co^{2+} and Ni^{2+} in $KMgF_3$ at 1.6 °K. Frequency is measured downwards from the no-phonon line.

$^4T_1$ term (some 1000 cm^{-1}) makes the Co^{2+} band appear much broader. The spectrum of Ni^{2+} is also shown in Fig. 2. As in V^{2+} and Ni^{2+}, measurements of the polarization of the Co^{2+} emission by uniaxial stress show that the bulk of the emission is magnetic dipole in character, and is associated with A_{1g} or E_g vibrations.

The fluorescent lifetime varies from 3.3 msec at 1.6 °K to 2.5 μsec at 550 °K. Even at the lowest temperatures nonradiative decay makes an important contribution (about $\frac{1}{3}$) to the inverse lifetime, and it is completely dominant at higher temperatures. The nonradiative decay rate is always in a conveniently measurable range, although it varies by nearly four orders of magnitude. It is this feature which makes the system $KMgF_3:Co^{2+}$ an attractive one to study. Very slow rates are difficult to disentangle from the much faster radiative decay,[4] while rates faster than 10^6 sec^{-1} require special equipment not readily available to us.

II. EXPERIMENT

A. Radiative and Nonradiative Lifetimes

The samples of $KMgF_3:Co^{2+}$ were those used in a previous study of the Jahn-Teller effect in the $^4T_2$ excited term.[6] Co^{2+} concentrations of 0.03 at 0.1 at.% were used. Over most of the temperature range both concentrations have identical lifetimes. Above 400 °K the fluorescence of the 0.03-at.% sample was too weak to measure, while below 77 °K the lifetime of the 0.1-at.% sample was perceptibly shorter. Furthermore, below 15 °K the apparent lifetime of the 0.1-at.% sample lengthened slightly, presumably because of radiation trapping. We have used only the 0.03-at.% data below 77 °K.

Fluorescence was excited by an argon-ion laser emitting about 1.3 W in all lines. The beam was chopped mechanically at 300 pulses per second. It was focused to a spot 10 μm across at the bevelled edge of the chopper, whose peripheral speed was 1100 cm/sec. The chopping time was measured to be 1.1 μsec. The fluorescent light was filtered to eliminate wavelengths less than 1.1 μm, and was detected with a cooled InSb detector, whose response time is less than 1 μsec; the signal was amplified by a low-impedance amplifier, with a bandpass of 0.1 Hz to 300 kHz. Below 300 °K, the signal-to-noise ratio was good enough to permit direct observation on an oscilloscope; above this a box-car integrator was used. A correction for the finite chopping time was applied to lifetimes of less than 10 μsec.

The reciprocal fluorescent lifetime w is plotted in Fig. 3 (full circles). It is the sum of the nonradiative and radiative decay rates, w_{NR} and w_R. The latter can be found, with the help of the Einstein relations, from the integrated no-phonon absorption in a sample of known concentration, and the observed ratio of the total emission rate

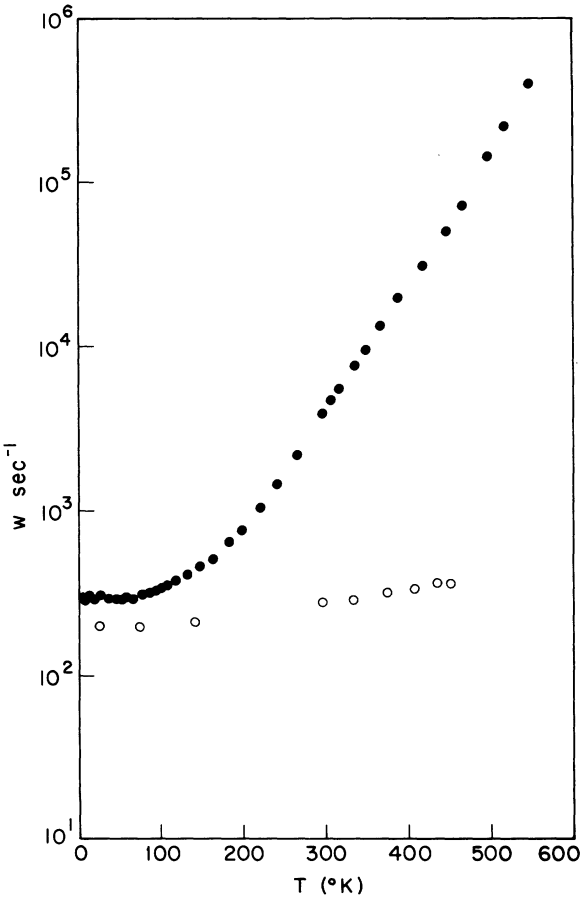

FIG. 3. Inverse lifetimes (decay rates) of the $^4T_2$ state of Co^{2+} in $KMgF_3$, as functions of temperature. Full circles: observed fluorescent decay rate w; open circles: radiative decay rate w_R (see text).

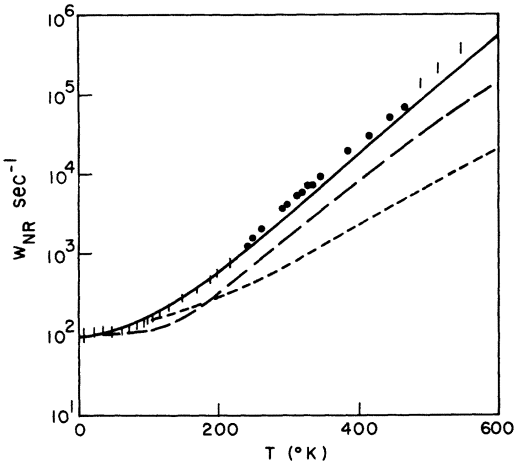

FIG. 4. Nonradiative decay rate of the $^4T_2$ state of Co^{2+} in $KMgF_3$. Circles and vertical bars: nonradiative decay rate deduced from the data of Fig. 3; full line: decay rate deduced from Eq. (16), with $S_0 = 2.0$, and the energy gap varying with temperature as observed; dotted line: the same with $S_0 = 2.0$, and the energy gap fixed at its 0 °K value; dashed line: Eq. (5), with $r = 18$, $S_0 = 2.0$.

to that in the no-phonon line. For one sample the integrated absorption $\int \alpha d\nu$ in the $^4T_1(\Gamma_6) \rightarrow {}^4T_2(\Gamma_6)$ no-phonon line was found to be 10 ± 1 cm^{-2}. Spin-resonance measurements on this sample gave a Co^{2+} concentration N of $(7 \pm 1.5) \times 10^{19}$ ions/cm^3. The Einstein relation for a magnetic dipole transition can be written[4]

$$w_{NP} = 8\pi \mu_r^2 \nu^2 (g_1/g_2) c \int_{NP} \sigma \, d\nu \quad . \tag{1}$$

Here w_{NP} is the emission rate in the no-phonon line, ν is the wave number in cm^{-1}, μ_r is the refractive index (1.4 for $KMgF_3$), $\sigma(\nu)$ is the absorption cross section $\alpha(\nu)/N$, and g_1/g_2 is the ratio of the upper- to the lower-state degeneracy. Equation (1) gives

$$w_{NP} = 11 \pm 2.5 \text{ sec}^{-1} \quad .$$

The ratio of the total emission (measured in photon, not energy, units) to that in the no-phonon line at 1.6 °K was found to be 21 ± 1. Thus the radiative decay rate at 1.6 °K is $w_R(1.6) = 230 \pm 50$ sec^{-1}.

This value of w_R is, as we shall see, rather larger than expected from purely magnetic dipole transitions. The discrepancy is due to phonon-induced electric dipole transitions. Thus w_R might be expected to increase somewhat with temperature. The temperature dependence is difficult to measure directly, since the no-phonon line ceases to be clearly distinguishable from the rest of the emission band above about 100 °K. Instead we measured the integrated $^4T_1 - {}^4T_2$ absorption as a function of temperature. Making the reasonable assumption that the temperature dependence of w_R is the same in emission and absorption, we obtain the values for w_R indicated by the open circles in Fig. 3.

The nonradiative decay rate w_{NR} given by $w_{NR} = w - w_R$, is plotted in Fig. 4. Only a representative selection of points below 100 °K is shown. Because of the uncertainty in the Co^{2+} concentration, w_R is less accurately known than w; hence w_{NR} is rather uncertain at low temperatures, as indicated by the error bars.

B. Temperature Shift of Energy Gap

Since the calculated nonradiative decay rate depends strongly on the energy gap, we need to know the gap as a function of temperature. The no-phonon line is not distinguishable above 100 °K, but we can find the change in its position with reasonable accuracy by measuring the shift of the centroid of the absorption band. If quadratic electron-lattice coupling is not important, so that there is no change in the average effective phonon frequency upon excitation of the Co^{2+} ion, the separation of the centroid from the no-phonon line should be independent of temperature.

We can estimate the contribution of quadratic coupling as follows: It can easily be shown by semiclassical arguments that the mean of the centroids of the absorption and emission bands, at 0 °K, differs from the no-phonon energy by an amount proportional to the quadratic coupling. The observed mean at 30 °K is 6935 ± 35 cm^{-1}, not significantly different from the no-phonon energy of 6920 cm^{-1}. The frequency shift on excitation must be less than 5%, producing a negligible shift of the band with temperature.

The centroid of the absorption band is plotted against temperature in Fig. 5. Part of the apparent shift is due to the redistribution of the population over the spin-orbit split levels of the ground state. The open circles in Fig. 5 show the result of correcting for this effect. The corrected shift is found to be proportional to the thermal dilatation of the lattice, $\delta l(T)/l$, as shown by the full line.[9] The proportionality constant is 7.5×10^4 cm^{-1} per unit dilatation.

This proportionality is to be expected if lattice anharmonicity is the cause of the shift. The proportionality constant can be predicted from the shift of the mean position of the no-phonon line under uniaxial stress, which is 0.46 cm^{-1} kg^{-1} mm^2.[6] Combining this with the known elastic constants of $KMgF_3$[10] gives a predicted shift of $3 \times 10^4 \delta l/l$ cm^{-1}. The observed shift is $2\frac{1}{2}$ times as large. Since we have eliminated quadratic coupling as an important contributor to the shift, we must suppose that the anharmonicity in the region

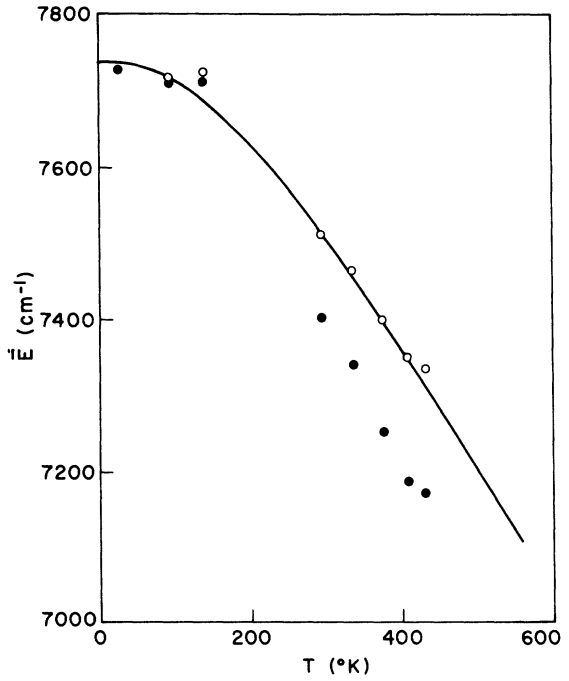

FIG. 5. Centroid of the $^4T_1 \rightarrow {}^4T_2$ absorption band as a function of temperature. Full circles: measured centroid; open circles: centroid corrected for the redistribution of population in the ground state; full line: the curve $\bar{E} = 7740 - 7.5 \times 10^4 \, (\delta l/l)$, where $\delta l/l$ is the thermal dilatation.

of the Co^{2+} ion is considerably larger than in the crystal as a whole.

III. THEORY OF MULTIPHONON TRANSITIONS

The rate w_{NR} of nonradiative transitions between two electronic states $|j\rangle$ and $|i\rangle$ separated by an energy $\hbar\Omega$ is given by the Golden Rule

$$w_{NR} = 8\pi^3 c^2 |M|^2 g(\Omega) \quad , \tag{2}$$

where $M = \langle i|\mathcal{H}|j\rangle$ in cm^{-1}, $g(\Omega)$ is the density of vibronic states in the final state, and $\mathcal{H}$ can be any operator which connects states i and j. In the present case, $\mathcal{H}$ represents the spin-orbit interaction. Vibronic coupling to nontotally symmetric modes will be shown to be less important for the transitions considered here. Chief interest centers on the calculation of $g(\Omega)$. We shall find that this is not a simple task, and requires many simplifying approximations.[11,12]

Two approximations which are basic to most calculations of $g(\Omega)$ are the following: (i) the system is harmonic, and (ii) the electron-phonon coupling is linear (i.e., there is no change in the vibrational frequencies as a result of the electronic transition, only a displacement of the origin of the vibrational coordinates). We will return to the question of the validity of these approximations later.

For the purposes of illustration, we begin with the hypothetical case of a single, discrete, totally symmetric vibrational mode of frequency ω_0. The vibronic spectrum associated with such a mode has the well-known "Pekarian" form at 0 °K[13]:

$$g(r) = e^{-S_0} S_0^r / r! \, . \tag{3}$$

Here r is the number of phonons emitted in the transition, so that for a nonradiative transition, $\Omega = r\omega_0$; S_0 is the Huang-Rhys parameter which specifies the strength of the electron-phonon coupling, and is equal to the mean number of phonons emitted in a radiative transition at 0 °K. Equation (3) describes a line spectrum, $g(r)$ being the normalized integrated strength of the rth vibronic. If we assume that each vibronic is broadened an amount of order ω_0, Eq. (3) becomes

$$g(\Omega) = e^{-S_0} S_0^r / \omega_0 \Gamma(r+1) \quad , \tag{4}$$

with $r = \Omega/\omega_0$. Equation (4) gives quite a good account of many observed spectra.

At finite temperatures, Eq. (3) is replaced by[14]

$$g(r) = (e^{-S_0} S_0^r / r!) F_r(T, S_0) \, , \tag{5}$$

where

$$F_r(T, S_0) = e^{-2S_0\bar{n}} r! \, S_0^{-r} (1+\bar{n}^{-1})^{r/2} I_r(2S_0[\bar{n}(\bar{n}+1)]^{1/2})$$

$$= e^{-2S_0\bar{n}} \sum_{l=0}^{\infty} \frac{r!}{l!\,(l+r)!} (1+\bar{n})^{l+r} (\bar{n} S_0^2)^l \, . \tag{6}$$

Here $I_r(y)$ is the modified Bessel function of order r, and $\bar{n} = (e^{\hbar\omega/kT} - 1)^{-1}$, the mean thermal occupation number of the vibrational mode. For small $\bar{n}$ and S_0, and large r, Eq. (6) reduces to

$$F_r = (1+\bar{n})^r \, , \tag{7}$$

which is the expression used by Riseberg and Moos.[3] Equation (7) has an obvious physical interpretation in terms of the induced and spontaneous emission of phonons, absorption and reemission being neglected.

This theory has been extended by Gummel and Lax[11] and by Pryce[12] to take the continuous nature of the phonon spectrum into account. We follow Pryce's formulation here. A phonon is described by an index α, a frequency ω_α, and a coupling coefficient a_α which represents the displacement of the origin of coordinates of the mode by the electronic transition. Then the effective phonon spectrum is

$$A_1(\omega) = \frac{1}{2} \sum_\alpha a_\alpha^2 \, \delta(\omega - \omega_\alpha) \, . \tag{8}$$

The Huang-Rhys parameter for this spectrum is

$$S_0 = \frac{1}{2} \sum a_\alpha^2 = \int_0^\infty A_1(\omega) \, d\omega \, . \tag{9}$$

Equation (4) is to be replaced by

$$g(\Omega) = e^{-S_0} \sum_{r=0}^{\infty} A_r(\Omega)/r! , \tag{10}$$

where $A_r(\Omega)$ is the result of convoluting $A_1(\omega)$ r times with itself:

$$A_r(\Omega) = \int_0^{\infty} A_{r-1}(\omega') A_1(\Omega - \omega')\, d\omega' . \tag{11}$$

At finite temperatures, Eq. (10) holds with $A_r(\omega)$ replaced by $B_r(\omega)$, where

$$B_1(\omega) = A_1(\omega)(1 - e^{-\hbar\omega/kT})^{-1} , \tag{12}$$

$$B_r(\Omega) = \int_{-\infty}^{\infty} B_{r-1}(\omega') B_1(\Omega - \omega')\, d\omega' ,$$

and $A_1(-\omega) \equiv -A_1(\omega)$. [Note that B_1 in Eq. (12) differs by a factor S from Pryce's definition.] Correspondingly, S_0 is replaced by $S(T)$, where

$$S(T) = \int_{-\infty}^{\infty} B_1(\omega)\, d\omega$$

$$= \int_0^{\infty} A_1(\omega) \coth(\hbar\omega/2kT)\, d\omega . \tag{13}$$

The convolutions in Eq. (11) can, in principle but with great labor, be done to arbitrary r; however, the problem can be greatly simplified and reduced to closed form by use of the central limit theorem. This tells us that for large r, $B_r(\Omega)$ can be approximated by a Gaussian:

$$B_r(\Omega) \sim (2\pi r y^2)^{-1/2} \exp[-(\Omega - rx)^2/2ry^2], \tag{14}$$

where

$$x = S^{-1} \int_{-\infty}^{\infty} \omega B_1(\omega)\, d\omega$$

and

$$y^2 = S_0^{-1} \int_{-\infty}^{\infty} \omega^2 B_1(\omega)\, d\omega - x^2 .$$

In terms of the effective phonon spectrum,

$$x = S_0\langle\omega\rangle/S ,$$

where

$$\langle\omega\rangle = S_0^{-1} \int_0^{\infty} \omega A_1(\omega)\, d\omega$$

and

$$y^2 = S^{-1} \int_0^{\infty} \omega^2 A_1(\omega) \coth(\hbar\omega/2kT)\, d\omega - x^2 . \tag{14a}$$

As T increases, x decreases steadily; y^2 initially decreases, but for $kT \gtrsim \hbar\langle\omega\rangle$ it levels off at a limiting value of about twice its 0 °K value. The high-temperature limits are

$$S(T \to \infty) = 2S_0\langle\omega^{-1}\rangle kT/\hbar ,$$

$$x(T \to \infty) = \hbar\langle\omega\rangle/2\langle\omega^{-1}\rangle kT, \tag{15}$$

$$y^2(T \to \infty) = \langle\omega\rangle/\langle\omega^{-1}\rangle - x^2 ,$$

where

$$\langle\omega^{-1}\rangle = S_0^{-1} \int_0^{\infty} \omega^{-1} A(\omega)\, d\omega .$$

For large r, the sum in Eq. (10) can be replaced by an integral. This integral is found to be[12]

$$g(\Omega) = \frac{\exp[-S + 1 + r_m + u(1 - u/r_m)x^2/y^2]}{\{\pi r_m[x^2 + 2y^2(1 + \ln r_m/S)]\}^{1/2}} , \tag{16}$$

where $u = \Omega/x$ and r_m is the solution of

$$u = r_m\{1 + 2[\ln(r_m/S) + r_m^{-1}]y^2/x^2\}^{1/2} . \tag{17}$$

[There is a typographical error in Pryce's expression equivalent to Eq. (17)]. In Eqs. (16) and (17), r_m is the value of r which makes the largest individual contribution to $g(\Omega)$. S is given by Eq. (13).

At low temperatures, for most reasonable $A_1(\omega)$, $x/y \sim 2$–4, and r_m approaches u if S_0 is not too large. At high temperatures y/x and S become large and proportional to T. In the high-temperature limit

$$r_m = S - 1 + x^2(u^2 - S^2)/2y^2 \quad (T \to \infty) ,$$

$$g(\Omega) = (2\pi S y^2)^{-1/2} \exp[-(\Omega - S_0\langle\omega\rangle)^2/2Sy^2] , \quad (T \to \infty) . \tag{18}$$

This is the classical result: a Gaussian centered at $S_0\langle\omega\rangle$ with dispersion $Sy^2 = 2S_0 kT\langle\omega\rangle/\hbar$. In this limit, S_0 and $\langle\omega\rangle$ only appear in the combination $S_0\langle\omega\rangle$, and $E_s = \hbar S_0\langle\omega\rangle$ is the stabilization energy due to the vibronic interaction in the excited state (E_s is just one-half of the Stokes shift). As one expects, the nature of the phonon spectrum is irrelevant in the classical limit.

Equation (18) can be written in a form more appropriate for nonradiative transitions:

$$g(\Omega) = \hbar(2\pi E_s kT)^{-1/2} e^{-E_A/kT} , \tag{19}$$

where $E_A = (\hbar\Omega - E_s)^2/4E_s$. Equation (19), when substituted in Eq. (2), gives the thermally activated nonradiative decay rate predicted by classical configuration coordinate arguments using a harmonic potential.[15]

Englman and Jortner[16] have shown that for sufficiently large S_0, Eq. (19) holds at all temperatures, with T replaced by T^*, where

$$T^* = (\hbar\omega/2k) \coth(\hbar\omega/2kT) . \tag{20}$$

This is the well-known "semiclassical" result.

IV. APPLICATION OF THEORY TO EXPERIMENT

In a static lattice, of cubic symmetry, the only operator connecting the $^4T_2$ and $^4T_1$ states is the spin-orbit interaction. Its squared matrix element, averaged over the substates of $^4T_2$ and summed over those of $^4T_1(F)$, is $\frac{25}{24}\zeta^2$ where ζ is the one-electron spin-orbit coupling parameter.[17] For Co^{2+} in $KMgF_3$, $\zeta = 500$ cm^{-1}.[6] Note that since this is an off-diagonal matrix element, it is not quenched by the dynamic Jahn-Teller effect.[18] Thus the spin-orbit contribution to $|M|^2$

in Eq. (2) is 2.6×10^5 cm^{-2}.

The contribution of symmetry-breaking vibrations to $|M|^2$ is[11]

$$|M_{\rm vib}|^2 = \frac{\hbar\bar{\omega}}{2\mu}\,\frac{|\langle {}^4T_1|V|{}^4T_2\rangle|^2}{\Omega^2}\ , \qquad (21)$$

where $\bar{\omega}$ is some average phonon frequency, μ is the ionic mass, and V represents the electron-phonon interaction. For the dominant E_g part of the interaction, $\langle {}^4T_1|V|{}^4T_2\rangle$ can be estimated from the known electron-lattice coupling in the ${}^4T_1$ and ${}^4T_2$ states[6,19] to be about 2000 cm^{-1} Å^{-1}, whence, for $\bar{\omega}/2\pi c = 300$ cm^{-1}, $|M_{\rm vib}|^2 \sim 100$ cm^{-2}. Thus the direct contribution of symmetry-breaking vibrations is negligible.

However, it would not be correct to leave symmetry-breaking out of the picture completely. We see from Fig. 3 that the lifetime changes by less than 5% as the temperature is raised from 1.6 to 50 °K. The nature of the initial state, on the other hand, changes drastically, since at 1.6 °K only the Γ_7 level of ${}^4T_2$ is populated, whereas at 50 °K the Γ_8^b level 10 cm^{-1} higher contains 60% of the population. Since $|M|^2$ is four times as large for the Γ_8 states as for Γ_6 or Γ_7,[17] and about 30% of the decay at 1.6 °K is nonradiative, we might have expected a 50% decrease in lifetime. The reason this does not happen, we believe, is that in a nonradiative transition the spin-orbit levels are thoroughly mixed up by the symmetry-breaking part of the electron-phonon interaction. The appropriate matrix element is $(\hbar/2\mu\bar{\omega})^{1/2}\langle {}^4T_2|V|{}^4T_2\rangle$, which is about 700 cm^{-1}.[6] This is much greater than the separation of the spin-orbit levels of ${}^4T_2$. For this reason we give $|M|^2$ its average value over all the spin-orbit levels, rather than its value for any particular level.

The ${}^4T_1$ term spreads over some 1000 cm^{-1} because of the spin-orbit interaction, and we have to decide what value of the energy gap $\hbar\Omega$ we should take. We have to remember that the initial state is strongly affected by the Jahn-Teller interaction.[6] Nonradiative transitions are taking place in a region of configuration-coordinate space where the E_g (Jahn-Teller) distortion is large. This distortion tends to quench the spin-orbit splitting of ${}^4T_1$.[18] The appropriate value of $\hbar\Omega$ is therefore the separation of the centroids of the ${}^4T_1$ and ${}^4T_2$ terms, rather than that of their nearest spin-orbit components. This separation is 6300 cm^{-1} at 0 °K.

We need a value for the Huang-Rhys parameter S_0. This is most easily obtained from the ratio of the strength of the no-phonon line to the total magnetic dipole transition strength. The latter can be calculated from the formula

$$w_{\rm MD} = \frac{8\pi^3}{3}\,\mu_\gamma^3\bar{\nu}^3\left(\frac{e^2\hbar}{m^2c^2}\right)\sum_i |\langle i|\vec{\mathbf{L}}+2\vec{\mathbf{S}}|j\rangle|^2\ , \qquad (22)$$

where μ_γ is the refractive index (1.4), and $\bar{\nu}$ is the mean wave number (in cm^{-1}) of the emission. The sum of matrix elements is calculated from the known[20] wave functions of Co^{2+} in $KMgF_3$ to be $14.5k^2$, where k is the orbital reduction factor, approximately 0.9 in $KMgF_3$.[21] This gives $w_{\rm MD} = 170\pm15$ sec^{-1}.

In absorption, one-half of the no-phonon strength is in $\Gamma_6\rightarrow\Gamma_6$ transition; the total emission rate in no-phonon lines is 22 ± 5 sec^{-1}. This is a fraction e^{-S_0} of the total magnetic dipole emission; hence $S_0 = 2.0\pm0.25$. While the temperature dependence of $w_{\rm NR}$ is not very sensitive to S_0, the absolute value is, and the 10% uncertainty in S_0 leads to an order of magnitude uncertainty in $w_{\rm NR}(0)$.

The next step is to obtain an effective one-phonon spectrum $A_1(\omega)$ from the observed vibronic sidebands. Because of overlapping transitions to different spin-orbit levels of ${}^4T_1$, it is difficult to extract this information from the Co^{2+} data. Figure 2 shows that the vibronic peaks are much the same for Ni^{2+} as for Co^{2+}, and we use the magnetic dipole part of the Ni^{2+} vibronic spectrum.[8] S_0 is sufficiently small (about 1.2) for Ni^{2+} for there to be no difficulty in deconvoluting the spectrum to obtain $A_1(\omega)$, shown in Fig. 6.

The temperature dependence of S/S_0, x and y^2, obtained by integrating Eqs. (13) and (14a) numerically, is shown in Fig. 7. (We note that the high-temperature limits, $S\propto T$, $x\propto T^{-1}$, $y^2\sim$ const, are all reached within our temperature range.) We substitute these parameters in Eqs. (16) and (17), with $S_0 = 2$ and $u = \Omega(T)/x$, where $\Omega(0) = 6300$ cm^{-1}

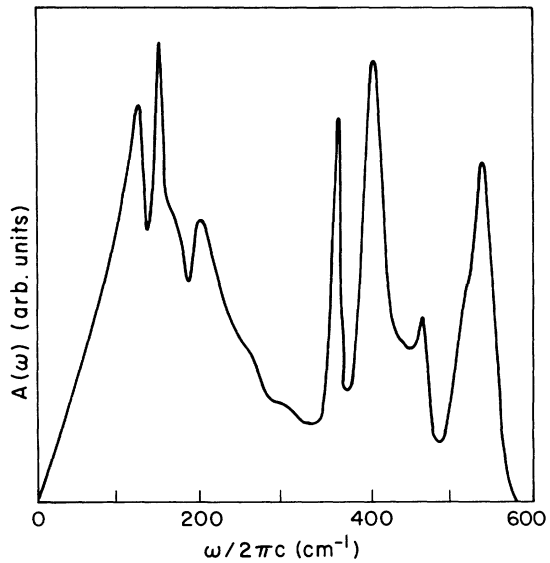

FIG. 6. Effective phonon spectrum $A_1(\omega)$ for Ni^{2+} in $KMgF_3$, deduced from the magnetic dipole phonon sidebands of the ${}^3T_2\rightarrow{}^3A_2$ emission.

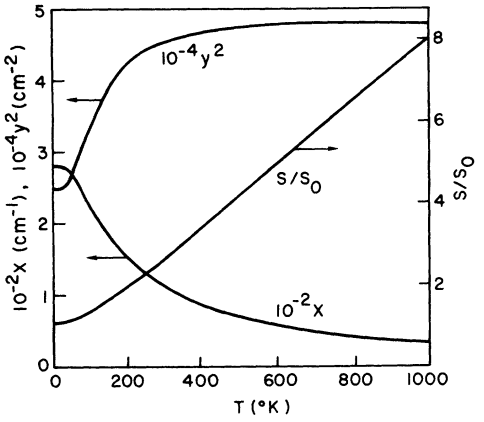

FIG. 7. Quantities $x(T)$, $y^2(T)$, and $S(T)/S_0$, deduced from the spectrum of Fig. 6.

and $\Omega(T)$ drops off with T according to the full line in Fig. 5. We obtain the full curve for $w_{NR}(T)$ given in Fig. 4. This curve has been normalized to the data at 0 °K; in fact the predicted value of $w_{NR}(0)$ for $S_0 = 2.0 \pm 0.25$ is in the range 10^3 to 5×10^4 sec^{-1}, compared with the observed value of about 100 sec^{-1}. This discrepancy is in direction expected for anharmonicity (see Sec. V).

In a strictly harmonic lattice, with linear electron-phonon coupling, there can be no shift of the energy gap with temperature. The result of taking Ω constant in Eq. (17) is shown by the dotted line in Fig. 4. There is a discrepancy of a factor of 30 at 550 °K. Clearly the bulk of the anharmonic effect is taken into account by our *ad hoc* procedure of giving Ω its observed variation with temperature.

It is of interest to compare the results of calculations using the continuum theory with those obtained from Eqs. (4)–(6), which are based on the assumption of a single effective vibrational frequency. With our parameters, Eq. (16) gives $2\pi c g(\Omega) = 3\times10^{-14}$ cm at 0 °K. This is close to the value obtained from Eq. (4) with an effective frequency $\omega_0/2\pi c = 350$ cm^{-1}, corresponding to $r = 18$. The temperature dependence of $g(\Omega)$, obtained from Eq. (6) for this value of r, is shown by the dashed curve in Fig. 4. Notice that this curve is for fixed Ω, and that above 100 °K it varies much faster than the corresponding curve (dotted) for the continuum. To match roughly the temperature dependence over the range 200–600 °K we need $r = 15$ or 16, corresponding to $\omega_0/2\pi c \simeq 400$ cm^{-1}.

Another effective frequency can be obtained by considering the "energy-gap law." In a wide range of organic molecules,[1] and also for rare-earth ions in crystals,[3] the nonradiative transition rate depends exponentially on energy gap: $w_{NR}(0) \propto e^{-A\Omega}$, for large Ω. Something like this is predicted by the single-frequency theory, since, if we use Stirling's formula for $r!$, Eq. (3) becomes

$$g(r) \propto (2\pi r)^{-1/2} \exp[-r(\ln r - \ln S_0 - 1)] \ , \qquad (23)$$

where $r = \Omega/\omega_0$. Since the preexponential term and the term in brackets are both slowly varying when $r \gg S_0$, the energy-gap law holds approximately, with

$$A = \omega_0^{-1}[\ln(r/S_0) - 1] \ . \qquad (24)$$

The results of using the continuum theory [Eq. (16)] are shown in Fig. 8, for three values of S_0. The energy gap law holds approximately, and is best for small S_0, as expected. An effective frequency can be found by substituting the slope at (say) $\Omega/2\pi c = 600$ cm^{-1} into Eq. (24). We find $\omega_0/2\pi c = 300$ cm^{-1}, independent (within ± 5%) of S_0. This is close to the mean frequency of the phonon spectrum used, which is 285 cm^{-1}.

Thus we obtain three different "effective" frequencies; roughly 300 cm^{-1} from the energy-gap law, 350 cm^{-1} from the absolute value of $g(\Omega)$, and 400 cm^{-1} from its temperature dependence. All of these are well below the maximum available phonon frequency, which is about 550 cm^{-1} (see Fig. 6). There is a widespread belief that only the high-frequency vibrations matter in multiphonon transitions.[1,3] This is thought to follow from the fact that the transition rate drops off rapidly with increasing r. Our calculations show that, for the parameters used here, this belief is mistaken.

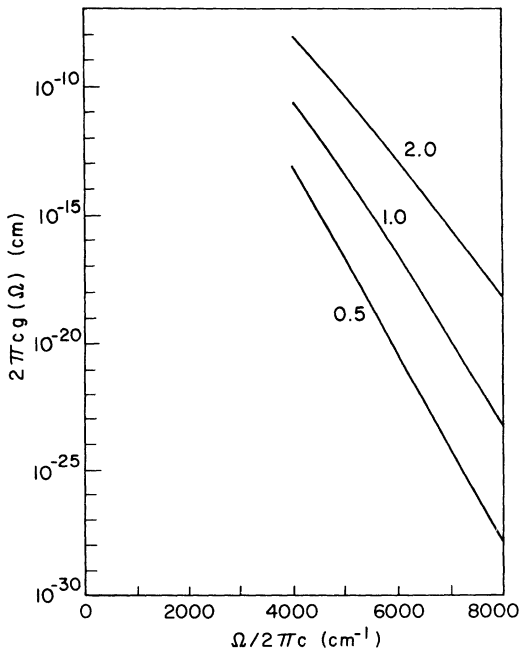

FIG. 8. "Energy-gap law" in the continuum model; $g(\Omega)$ for $T = 0$, calculated from Eq. (16) for three values of S_0, plotted against $\Omega/2\pi c$.

V. EFFECT OF ANHARMONICITY ON VIBRATIONAL OVERLAP

The dominant contribution to the overlap integral comes from regions of configuration coordinate space very far from the origin. We might expect, therefore, that anharmonicity should have a large effect on the integral. While it is not practicable to calculate this for a solid, we can get a feeling for the effect of anharmonicity by considering a diatomic molecule at 0 °K.

We assume that we have a diatomic molecule with two electronic states. In the ground state, the nuclei move in a Morse potential[22]:

$$V(q) = \hbar\omega(1 - e^{-aq})^2/2a^2 \quad . \tag{25}$$

Here ω is the classical frequency of small vibrations; q is the displacement, measured from its equilibrium position, in units of $(\hbar/\mu\omega)^{1/2}$, where μ is the reduced mass; $\hbar\omega/2a^2$ is the dissociation energy. We assume for simplicity that Eq. (25) also holds in the excited state, with q replaced by $q - q_0$ and V by $V - \hbar\Omega$, where

$$\Omega/\omega = r - \tfrac{1}{2}a^2(r+\tfrac{1}{2})^2 \quad .$$

Then,

$$S_0 = \tfrac{1}{2}q_0^2$$

and

$$g(r) = |\langle 0|r\rangle|^2 \quad .$$

The overlap integral is given by[23]

$$\langle 0|r\rangle = (-1)^r N_r e^{-px}(1+\delta)^{p-r}\sum_{m=1}^{r} C_r^m \delta^m \quad . \tag{26}$$

Here $N_r^2 = \binom{p}{r}(1 - 2r/p)$, $p = 2a^{-2} - 1$, $x = aq_0/2$, $\delta = -\tanh x$, and

$$C_r^m = \binom{r}{m}\binom{p-1}{r-m}^{-1}\sum_{k=0}^{r-m}(-1)^k\binom{r-m}{k}\binom{p-k-1}{r-1} \quad . \tag{27}$$

It is essential that the sum in Eq. (27) be evaluated algebraically, since for large r and p there is gross cancellation, roughly r significant figures being lost on numerical summation. The sums for $r \leq 3$ are given by Jarmain and Fraser.[24] A general formula can be obtained with the aid of the identity[25]

$$\sum_{k=0}^{l}(-1)^k\binom{l}{k}\binom{i-k}{j} = \binom{i-l}{i-j} \quad , \tag{28}$$

whence

$$C_r^m = \binom{r}{m}\binom{r-1}{m-1}\binom{p-1}{r-m}^{-1} \quad . \tag{29}$$

Diatomic fluorides of divalent metals all have dissociation energies of roughly $50\hbar\omega$,[26] so we take $a = 0.1$. With $S_0 = 2$ and q_0 positive, we obtain

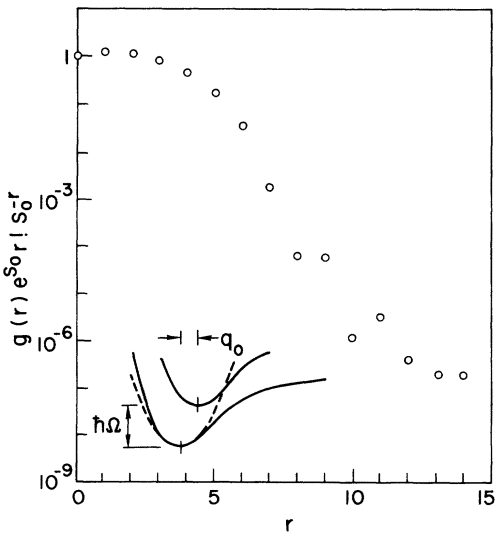

FIG. 9. Effect of anharmonicity on the overlap factor of a Morse oscillator. The ordinate is the ratio of $g(r)$ to its harmonic value. Insert: schematic configuration coordinate diagram for $q_0 > 0$; full lines: Morse oscillator; dotted lines: harmonic oscillator. For $q_0 > 0$, the important region of overlap is $q > q_0$, and the overlap is decreased by anharmonicity. For $q_0 < 0$, the important region is $q < q_0$, and the overlap is increased by anharmonicity.

the values of $g(r)$ (expressed in units of the corresponding harmonic value, $e^{-S_0}S_0^r/r!$) shown in Fig. 9. The rapid falloff as r increases is a consequence of the fact that for $q_0 > 0$ the Morse curves are more widely separated in the region of overlap than the corresponding parabolas (see insert in Fig. 9). Thus we might expect multiphonon transitions with $r \sim 15$ to be a factor $\sim 10^{-7}$ slower than calculated from the harmonic approximation. The effect is likely to be less pronounced in a solid, where the potential curves cannot possibly be as flat as Morse curves at large displacements. The observed rate in $KMgF_3$:Co, $\sim 10^{-2}$ slower than calculated, is perhaps reasonable.

A long-standing puzzle in this field has been the nonradiative $^2E \rightarrow {}^4A_2$ decay rate of ruby (Al_2O_3:Cr^{3+}). This transition is weakly coupled to the lattice, with $S_0 \lesssim 0.25$. In the harmonic approximation, $w_{NR} \sim 2\pi(\xi^2/\hbar^2\omega)e^{-S_0}S_0^r/r!$ and with $S_0 = 0.25$, $r = 20$, this gives $w_{NR} \sim 10^{-16}$ sec^{-1}. The observed rate at low temperatures is 26 sec^{-1}.[4] For this transition q_0 is negative, since the energy gap decreases under hydrostatic compression.[27] For negative q_0 with the above values of S_0 and r, Eq. (24) predicts the value of $|\langle 0|r\rangle|^2$ to be 10^{19} times its harmonic value, more than enough to account for the discrepancy.

This calculation confirms the assertion of Makshantsev[28] that anharmonic effects can have an

enormous effect on nonradiative decay in a diatomic molecule. We do not claim that it is quantitatively applicable to solids, even as to order of magnitude. However, it does confirm one's intuitive judgement, that the decay rate is decreased by anharmonicity if q_0 is positive, corresponding to an increase in the equilibrium internuclear distance in the excited state, and increased if q_0 is negative.

VI. CONCLUSIONS

We have set out to test how well the harmonic continuum theory of multiphonon vibronic transitions can account for the nonradiative decay of the $^4T_2$ excited state of Co^{2+} in $KMgF_3$. In this theory anharmonic effects and quadratic coupling are neglected, and the phonon spectrum is characterized by two parameters, the mean frequency and the dispersion. We find that the temperature dependence of the nonradiative decay rate w_{NR} can be accounted for over nearly four orders of magnitude, provided that we take anharmonic effects into account by giving the energy gap its observed dependence on temperature. The absolute value of w_{NR} is not correctly predicted, but the deviation is in the direction expected for anharmonicity. Anharmonic effects may also account for the enormous discrepancy between theory and experiment in the nonradiative decay of the ^2E state of ruby.

ACKNOWLEDGMENTS

I am most grateful to H. M. O'Bryan for measuring the thermal expansion of $KMgF_3$; to H. J. Guggenheim for providing the crystals; to R. Englman, M. Lax, and J. Van der Ziel for helpful discussions; to B. F. Levine, F. R. Merritt, and J. Van der Ziel for the loan of equipment; and to E. A. Sadowski for help with the experiments.

[1] *Proceedings of the Twentieth Réunion Annuelle, Société de Chimie Physique, Paris, 1969,* special issue of J. Chim. Phys. (1970); R. Englman and B. Barnett, J. Lumin 3, 37 (1970); S. H. Lin, J. Chem. Phys. **56**, 2648 (1972); A. Nitzan and J. Jortner, J. Chem. Phys. **56**, 2079 (1972); J. Chem. Phys. **56**, 3360 (1972), and references therein, F. K. Fong, S. L. Naberhuis, and M. M. Miller, J. Chem. Phys. 56, 4020 (1972).

[2] M. D. Sturge, H. J. Guggenheim, and M. H. L. Pryce, Phys. Rev. B **2**, 2459 (1970).

[3] L. A. Riseberg and H. W. Moos, Phys. Rev. **147**, 429 (1968); H. W. Moos, J. Lumin. **1**, 106 (1970).

[4] D. F. Nelson and M. D. Sturge, Phys. Rev. 137, A1117 (1965).

[5] B. di Bartolo and R. Peccei, Phys. Rev. 137, A1770 (1965); P. Kisliuk and C.A. Moore, Phys. Rev. **160**, 307 (1967); B. di Bartolo and R. C. Powell, Nuovo Cimento B **66**, 21 (1970).

[6] M. D. Sturge and H. J. Guggenheim, Phys. Rev. B **4**, 2092 (1971).

[7] L. F. Johnson, H. J. Guggenheim, and R. A. Thomas, Phys. Rev. **149**, 179 (1966).

[8] M. D. Sturge, Solid State Commun. **9**, 899 (1971).

[9] The thermal expansion of a single crystal of $KMgF_3$ was measured along the ⟨001⟩ direction by H. M. O'Bryan (private communication) using the dilatometer method. The dilation is given by $\delta l/l = \int_0^T \alpha\, dT$, where α is found to fit the Grüneisen equation: $\alpha = C_v(T/\Theta)/3Q_0(1+kU/Q_0)^2$, with $\theta = 450$ °K, $Q_0 = 450$ kcal/mole, $k \sim 3$. Here $C_v(T/\Theta)$ is the Debye molar specific heat and $U = \int_0^T C_v\, dT$.

[10] H. M. Rosenberg and J. K. Wigmore, Phys. Lett. A **24**, 317 (1967).

[11] H. Gummel and M. Lax, Ann. Phys. (N. Y.) 2, 28 (1957).

[12] M. H. L. Pryce, in *Phonons*, edited by R. W. H. Stevenson (Plenum, New York, 1966), p. 403.

[13] J. J. Markham, Rev. Mod. Phys. **31**, 956 (1959).

[14] K. K. Rebane, *Impurity Spectra of Solids* {(Nauka, Moscow, 1968) [English translation: Plenum, New York, 1970]} Eq. 13.10.

[15] C. C. Klick and J. H. Schulman, in *Advances in Solid State Physics*, edited by F. Seitz and D. Turnbull (Academic, New York, 1957), Vol. 5, p. 97.

[16] R. Englman and J. Jortner, Mol. Phys. **18**, 145 (1970).

[17] J. C. Eisenstein, J. Chem. Phys. **34**, 1628 (1961).

[18] F. S. Ham, Phys. Rev. 138, A1727 (1965).

[19] J. K. Wigmore, H. M. Rosenberg, and D. K. Garrod, J. Appl. Phys. **39**, 682 (1968).

[20] A. D. Liehr, J. Phys. Chem. **67**, 1314 (1963).

[21] J. H. M. Thornley, C. G. Windsor, and J. Owen, Proc. R. Soc. A **284**, 252 (1965).

[22] P. M. Morse, Phys. Rev. **34**, 57 (1929).

[23] P. A. Fraser and W. R. Jarmain, Proc. Phys. Soc. Lond. A **66**, 1145 (1953).

[24] W. R. Jarmain and P. A. Fraser, Proc. Phys. Soc. Lond. A **66**, 1153 (1953).

[25] J. Riordan, *Combinatorial Identities* (Wiley, New York, 1968), p. 8.

[26] G. Herzberg, *Spectra of Diatomic Molecules*, 2nd ed. (Van Nostrand, Princeton, N.J., 1950).

[27] A. L. Schawlow, A. H. Piksis, and S. Sugano, Phys. Rev. **122**, 1469 (1961).

[28] B. I. Makshantsev, Opt. Spektrosk. **31**, 355 (1971) [Opt. Spectrosc. **31**, 191 (1971)].